Mechanics of Advanced Materials and Structures

ISSN: 1537-6494 (Print) 1537-6532 (Online) Journal homepage: http://www.tandfonline.com/loi/umcm20

An investigation into the flexural and drawing behaviors of GFRP-based fiber–metal laminate

Ali Rajabi, Mehran Kadkhodayan & Sadegh Ghanei

To cite this article: Ali Rajabi, Mehran Kadkhodayan & Sadegh Ghanei (2018) An investigation into the flexural and drawing behaviors of GFRP-based fiber–metal laminate, Mechanics of Advanced Materials and Structures, 25:10, 805-812, DOI: 10.1080/15376494.2017.1308587

To link to this article: https://doi.org/10.1080/15376494.2017.1308587

Accepted author version posted online: 23 Mar 2017.
Published online: 27 Apr 2017.

MECHANICS OF ADVANCED MATERIALS AND STRUCTURES
2018, VOL. 25, NO. 10, 805–812
https://doi.org/10.1080/15376494.2017.1308587

Taylor & Francis
Taylor & Francis Group

ORIGINAL ARTICLE

An investigation into the flexural and drawing behaviors of GFRP-based fiber–metal laminate

Ali Rajabi[a], Mehran Kadkhodayan[a], and Sadegh Ghanei[b]

[a]Department of Mechanical Engineering, Ferdowsi University of Mashhad, Mashhad, Iran; [b]Department of Materials Engineering, Ferdowsi University of Mashhad, Mashhad, Iran

ABSTRACT

Fiber–metal laminates (FMLs) are advanced composite materials that consist of bonded thin metal sheets and fiber-reinforced composite layers. In this article, mechanical behavior of a thermoplastic-based FML is investigated, which is composed of glass-fiber-reinforced polypropylene (GFRP) laminate and aluminum AA1200-O as the core and skin layers, respectively. Engineering constants of the composite laminate were achieved using Timoshenko's beam theory, flexural and tensile test results. Finite element simulations of the GFRP-based FML were performed to predict the behavior of this material in three-point bending and deep drawing tests. Some experimental verification tests were conducted to prove the reliability of results in the FE analysis of the FML. Comparison of the results shows an excellent correlation between the FE analysis and experimental tests.

ARTICLE HISTORY
Received 11 October 2013
Accepted 15 March 2017

KEYWORDS
Fiber–metal laminate; finite element analysis; mechanical behavior; thermoplastic

1. Introduction

One of the most popular composite materials, known as fiber–metal laminate (FML), is used in industries to develop lightweight structures. These laminates gather the good properties of metals, such as ductility, impact, damage tolerances and surface finish with the advantages of fiber composite materials, such as high-specific strength, high-specific stiffness, good corrosion and fatigue resistance. These excellent properties convert them to a good substitute for metal structures, especially in automotive and aerospace industries.

The first generation of the FMLs was based on the composites with epoxy thermosetting polymer matrices, but their brittleness and problems in manufacturing led to an increased interest in development and utilization of the FMLs with thermoplastic-based composites. Thermoplastic fiber–metal laminates (TFMLs) offer an excellent combination of mechanical properties as well as rapid and low-cost production of structural components [1, 2].

Mechanical properties of the TFML systems have been investigated in a number of previous studies. Carrillo and Cantwell [3] conducted a series of tensile tests on a new type of TFML and their results showed that the FML offers a higher strength than that of the plain thermoplastic composite and the strain to failure of the FML is much greater than that of the plain aluminum alloy. The effect of fiber orientation on the tensile properties of the FMLs was also studied by Moussavi-Torshizi et al. [4] in which their results expressed that fibers with zero orientation in laminate improve modulus of elasticity, yield stress and ultimate tensile stress, considerably. Khalili et al. [5] used stainless steel layers in their GRP composites. The bending stiffness of their FML showed an increase of 16 times and the displacement under the point of loading showed an increase of nearly 4 times compared to the GRP composite. Research on drawing behavior of metal–composite sandwich structures by Gresham et al. [6] showed the effect of constituent material properties and the process variables on the formability of FML systems. Lin et al. [7] studied the carbon-reinforced aluminum laminates with superior fatigue crack growth resistance. They explained that the fatigue crack growth rate of their FMLs was about two orders of magnitude lower than that of aluminum alloy. Moreover, the study of crack growth resistance revealed that the capacity of slow stable tearing prior to rapid fracture in the FMLs was as it can be seen in metals [8].

In the last few decades, the finite element method (FEM) has become the prevalent technique successfully used for the design and analysis of mechanical behavior of the composite materials and the composite structures [9]. However, few numerical researches have been done on the FMLs using the FEM. For instance, spring back evaluation of the FMLs during forming process [10], failure of the FMLs subjected to the low-velocity impact loading [11], investigation of stamp forming [12], damage evolution and prediction of the burst strength of the cylindrical FMLs used for storage vessel [13], and failure prediction of the FMLs subjected to the shear test [14] have been the subjects of the FEM studies of the FMLs.

The main aim of the current study is to investigate the flexural and drawing behaviors of the glass-fiber-reinforced polypropylene (GFRP)-based FML using FE simulations and experimental verifications. The multi-layers and nonisotropic nature of the FMLs makes the FE analysis difficult. At the first step of

CONTACT Mehran Kadkhodayan kadkhoda@um.ac.ir Department of Mechanical Engineering, Ferdowsi University of Mashhad, Vakil-abad Street, 91775-1111 Mashhad, Iran.
Color versions of one or more figures in this article are available online at www.tandfonline.com/umcm.

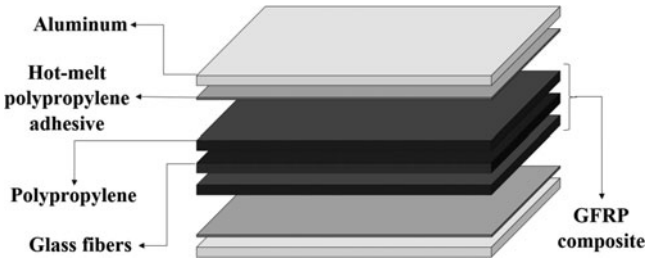

Figure 1. Schematic illustration of the GFRP-based FML lay-up.

the present study, a method is introduced for determination of directional properties of the GFRP-based FML as an orthotropic material. Then, the obtained directional properties of the FMLs are used to investigate their mechanical (flexural and drawing) behaviors, numerically. Finally, the consistency of numerical and experimental results is studied.

2. Materials processing and characterization

2.1. *Laminate preparation*

The materials used in the present study to manufacture the GFRP-based FML, included aluminum 1200-O, polypropylene, hot-melt polypropylene adhesive (PP-g-MAH) and woven glass-fibers [0/90]. The thermoplastic FML was manufactured based on the GFRP laminate and aluminum AA1200-O as the composite and metal layers, respectively. The thickness of aluminum was 0.5 mm and the composite laminate had a thickness of 1 mm. To manufacture the GFRP laminate, a hot plate press was used; two polypropylene sheets were stacked and fibers were placed between them. The composite core was sandwiched between two layers of cleaned aluminum sheet by applying a 0.2 mm thick layer of a hot-melt polypropylene adhesive that was placed at each bi-material interface, as shown in Figure 1. The laminate was consolidated by heating to 200°C in the hot plate press for 10 min.

2.2. *Materials characterization*

2.2.1. *Tensile properties*

The flat tensile specimens were fabricated according to the ASTM: E8M for aluminum and ASTM: D3039 for polypropylene, fiber-reinforced polymer composite and FML. Tensile tests were conducted using Zwick/Z250 testing machine as explained in the ASTM Standards.

Average of at least three specimens has been reported for each kind of specimen. The mechanical properties of the mentioned materials, including longitudinal elastic modulus, ultimate tensile stress and final elongation are shown in Table 1. Full annealed aluminum sheet showed isotropic behavior during tensile tests. Furthermore, the GFRP was a woven composite material with the same density in two directions; therefore, it was considered as an orthotropic laminate. Due to anisotropic behavior of composite laminate, the longitudinal elastic modulus is presented in Table 1 instead of elastic modulus of isotropic material. The longitudinal elastic modulus is the slope of linear elastic part of the stress-strain curve of a material in longitudinal direction. Figure 2 shows the stress-strain curves of aluminum 1200-O and GFRP laminate, which are required for FE simulations and polypropylene curve, which is needed to obtain other mechanical properties of GFRP laminate. As shown in the figure, the linear elastic parts of these curves were estimated with three linear polynomials and their slopes were reported as longitudinal elastic modulus in Table 1.

2.2.2. *Shear modulus and Poisson's ratio*

An orthotropic materials such as FMLs show different responses to stress and strain when tested in different directions. In this study, the longitudinal and transverse moduli of elasticity, three shear moduli and Poisson's ratio are needed for bending and drawing simulations of the FML. As mentioned, the longitudinal modulus of elasticity was found from tensile test and to evaluate the shear modulus of material the three-point bending test was used. This test method for a rectangular cross-section isotropic beam based on well-known Timoshenko's beam theory is given by the following equation:

$$w = \frac{PL^3}{4Ebh^3} + \frac{PL}{4K_sGbh}, \tag{1}$$

where w is the central deflection, P is the applied load, L is the span, b is the width, h is the thickness, and E and G are the elastic and shear moduli, respectively. The parameter k_s is the so-called *shear correction factor* or *shear coefficient*, for adjustment the shear stress distribution that is not uniform through the thickness of the beam. According to previous researches, $k_s \approx 5/6 = 0.833$ [15].

Since the GFRP beam is composed of an orthotropic material, there is no coupling between shear and normal stresses. Furthermore, the variation in the Poisson's ratio between layers would lead to a violation of the plane stress assumption. Nevertheless, this conditions using Eq. (1) is an extension of the conditions originally used by Timoshenko, who limited his analysis to plane stress beams composed of a single isotropic material [16, 17]. If the longitudinal axis of the beam coincides with the fiber direction, E equals E_{11} and G coincides with G_{13}. Eq. (1) is obtained with the assumption that the anticlastic curvature in the 1–2 plane due to the Poisson's effect is negligible, which actually occurs when the beam width is small compared to L. When this condition is not satisfied, the plate theory must be addressed, resulting in the replacement of E_{11} with the quantity $E_{11}/(1-\nu_{12}\nu_{21})$, in the analytic solution [18].

In order to find E_{11} and G_{13}, It is convenient to rewrite Eq. (1) in the following form by dividing both sides of the equation

Table 1. Mechanical properties of the GFRP-based FML and their corresponding constituents.

	GFRP-based FML	Glass-fiber-reinforced polypropylene	Aluminum 1200-O	Polypropylene
Ultimate tensile stress S_{ut} (MPa)	50	36.7	90	20
Longitudinal elastic modulus E_{11} (GPa)	30	0.94	68.5	0.3

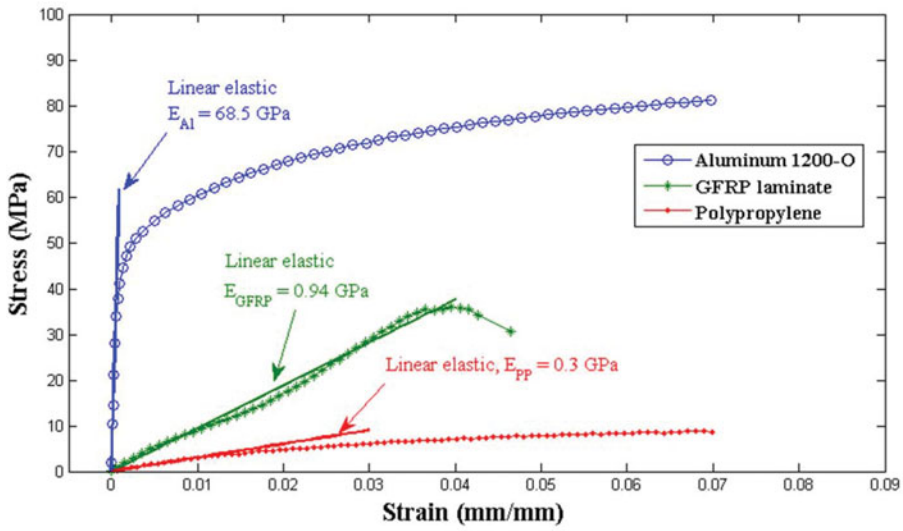

Figure 2. Engineering tensile stress-strain curves and estimated linear polynomials on the elastic parts of aluminum 1200-O, GFRP laminate and polypropylene.

by $\frac{PL^3}{4bh^3}$

$$\frac{1}{E_f} = \frac{1}{E_{11}} + \frac{1}{K_s G_{13}} \left(\frac{h}{L}\right)^2, \tag{2}$$

where:

$$E_f = \frac{L^3}{48I} \left(\frac{P}{w}\right). \tag{3}$$

In the Eqs. (2) and (3), E_f is the apparent modulus of elasticity, L is the span, I is the second moment of area and P/w is the slope of load–deflection curve.

To determine the shear modulus and the true modulus of elasticity, several three-point bending tests with different widths and spans were performed on the GFRP samples. The widths of samples were 12, 16, 16.5 and 17 mm and the following spans were 29, 27, 20, and 49 mm. Plotting the quantity $1/E_f$ against $(h/L)^2$ and linear regression of data would result in a first-degree polynomial. The slope modified by the shape factor, and the intercept with the y-axis would provide the shear modulus and the true modulus of elasticity, respectively, Figure 3. Putting $k_s = 0.833$ in Eq. (2), the solid line in the figure gave $E_{11} = 1.08$ GPa and $G_{13} = 34$ MPa.

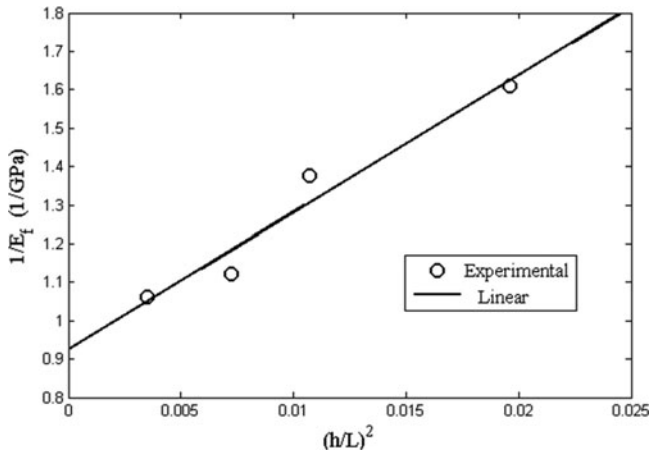

Figure 3. Graphical solution for shear modulus and true modulus of elasticity.

The elastic constants for GFRP lamina used in FE simulations are shown in Table 2. As mentioned, the GFRP is a polypropylene-based composite with the woven glass fiber with the same density in two directions, thus E_{11}, G_{13} and ν_{12} will be equal to E_{22}, G_{23} and ν_{21}, respectively. After determination of E_{11}, E_{22}, G_{13} and G_{23} to obtain Poisson's ratio ν_{12}, the longitudinal modulus E_{11} is replaced by the quantity $E_{11}/(1 - \nu_{12}\nu_{21})$ in Eq. (2). The E_{11} in the numerator of the fraction of $E_{11}/(1 - \nu_{12}\nu_{21})$ is substituted by the longitudinal modulus in Table 1 ($E_{11} = 940$ MPa) obtained from tensile test. Solution of the relation $0.94/(1-\nu_{12}\nu_{21}) = 1.08$ would result $\nu_{12} = 0.36$.

When the woven-glass-reinforced lamina with the same density in two directions is loaded in shear within the 1–2 plane, all the layers are deformed in parallel, and the well-known rule-of-mixtures holds:

$$G_{12} = G_{glass} \frac{t_{glass}}{t} + G_{pp} \frac{2t_{pp}}{t}, \tag{4}$$

where G_{12} is the same with the inplane shear modulus of the unidirectional layer having a fiber volume fraction equal to that of cloth-reinforced layer [19]. G_{glass}, G_{pp} are shear modulus and t_{glass}, t_{pp} are thickness of fiber-glass-reinforced and polypropylene respectively; and t is the total thickness of lamina. As show in Figure 4, $t_{glass} = 0.5t$, $t_{pp} = 0.25t$. The shear modulus along the 1–3 plane is easily derived from micromechanics:

$$\frac{1}{G_{13}} = \frac{t_{glass}}{tG_{glass}} + \frac{2t_{pp}}{tG_{pp}}. \tag{5}$$

In the Eq. (5), the value of G_{pp} is calculated with using $\nu = 0.3$, from the Eq. (6) for isotropic materials:

$$G_{pp} = \frac{E_{pp}}{2(1+\nu)}. \tag{6}$$

If the experimental G_{13} given by the bending tests and $G_{pp} = 115$ MPa is substituted in Eq. (5), $G_{glass} = 20$ MPa and as a result $G_{12} = 83$ MPa is derived from Eq (4).

Table 2. Mechanical properties of the GFRP laminate used in finite element modeling.

Material	E_{11} (MPa)	E_{22} (MPa)	G_{12} (MPa)	G_{13} (MPa)	G_{23} (MPa)	υ_{12}
Glass-fiber-reinforced polypropylene	940	940	83	34	34	0.36

3. Finite element analysis

3.1. *FE model of bending*

To investigate bending behavior of the GFRP-based FML numerically; the commercial finite element software, ABAQUS, was used. The dimensions of the FML and test set up were considered according to the ASTM: D790. Dynamic explicit method was used for bending simulation of the FML sample.

Figure 5 shows the FE model in contrast with the real experimental set up of the FML bending. From the figure, three layers of the model are apparent. The upper and lower layers were modeled as aluminum and the middle layer was modeled as GFRP composite. Because of using full-annealed aluminum sheet it was assumed that the aluminum had no anisotropy and obeyed isotropic hardening rule during simulations. Furthermore, the hardening behavior of aluminum was considered using true stress-strain curve derived from engineering stress-strain curve in Figure 2. The GFRP laminate was modeled as an orthotropic composite material and proper anisotropy was considered. Directional properties of the GFRP laminate, including longitudinal and transverse moduli of elasticity, three shear moduli and Poisson's ratio were obtained in Section 2.2. It can be shown that the composite material does not leave elastic part of its stress-strain curve during simulation. In this model, adhesive layer was ignored because the mechanical properties of hot-melt polypropylene adhesive were very similar to the matrix of composite layer. Moreover, when no slip occurred between the sheet metal faces and the composite core, this assumption does not make any considerable error [20].

It was assumed that the contact property between the sample, nose and support surfaces obeyed the Coulomb's law and the experimentally obtained frictional coefficient of 0.1 was used. As shown in Figure 5, the loading nose and supports had cylindrical surfaces in which the radii of supports and loading nose were 5 mm, and support span was 26 mm. To reduce the computation time, the nose and the supports were assumed to be rigid parts and they were meshed with 3-D bilinear rigid quadrilateral elements. In this model, 100 elements along the longitudinal and five elements in the thickness directions were intended. The type of elements was SC8R with settings (quadrilateral inplane continuum shell, reduced integration with hourglass control and finite membrane strains). The boundary conditions of supports were fully constrained and the nose was constrained except in the vertical direction.

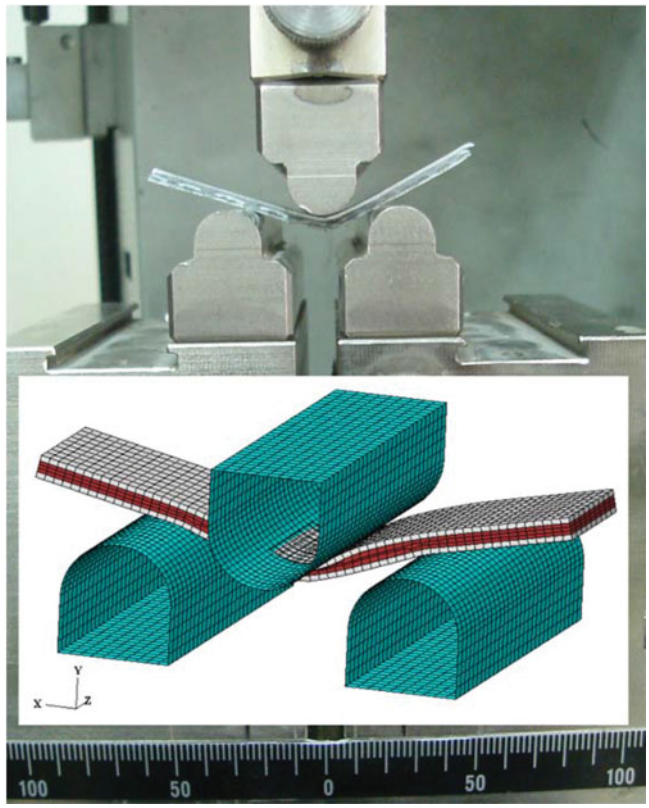

Figure 5. Finite element model of the GFRP-based FML for three-point bending test in contrast with real set up.

3.2. *FE model of deep drawing*

A three-ply circular sandwich sheet composed of aluminum AA1200-O as face sheets and the GFRP laminate as central material was considered as blank sheet. The diameter and thickness of blank sheet were 110 mm and 2 mm, respectively. The dimensions of die parts are shown in Table 3. The required mechanical properties and hardening rules used in the simulation of deep drawing were similar to the bending simulation of the FML. Due to the existence of wrinkling, the problem is not axisymmetric and a 3-D model must be applied. Figure 6 shows the FEM for the analysis of the deep drawing process in contrast with the experimental set up (the FML is represented as the yellow part). Wrinkling is a type of local instability that occurs in the deep drawing of a blank sheet. The model used for wrinkling analysis of a circular sheet must provide for switching to the buckling mode of the sheet. The first stage in the simulation was

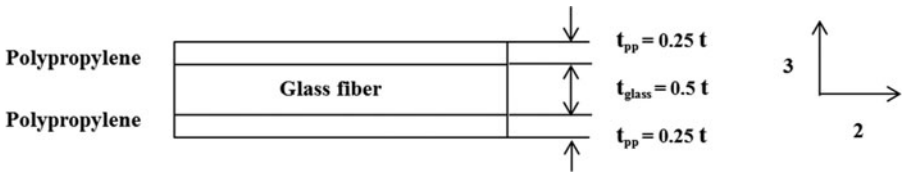

Figure 4. Modeling of the GFRP lamina.

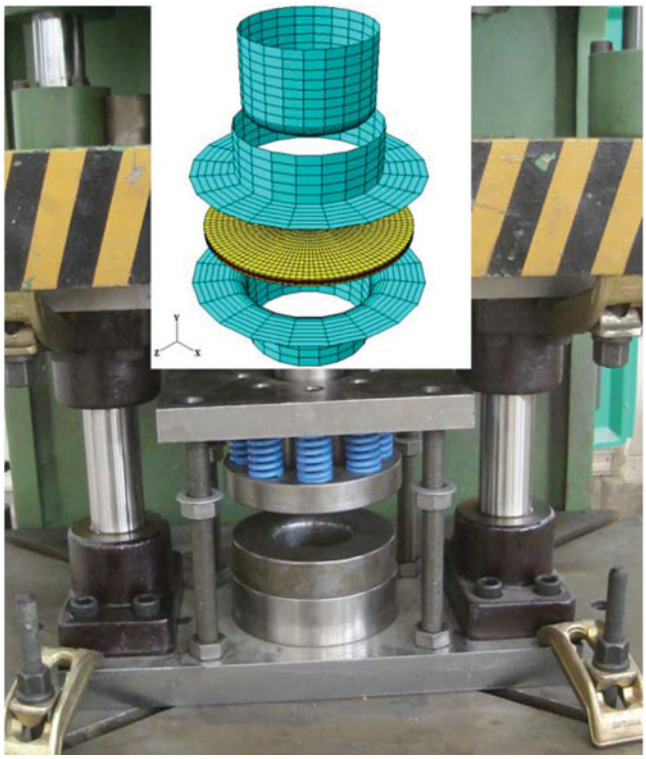

Figure 6. Experimental and finite element set ups of the deep drawing test.

a linear eigenvalue buckling analysis to estimates the buckling modes. Afterwards, the second stage involved introducing a slight initial geometric imperfection in the sheet. A single mode or a combination of modes was used to construct the imperfection. Eventually, the final stage of the analysis simulated the post-buckling response of the sheet for a given imperfection [21]. In this study, the buckling modes of the blank sheet were computed by running a linear buckling analysis in ABAQUS/standard and these modes were stored in the results file. Subsequently, the imperfection option in ABAQUS/explicit was used to read the buckling modes corresponding to the lowest eigenvalue, after scaling; they were used to perturb the nodal coordinates of the sheet.

Dynamic explicit analysis of deep drawing in this simulation contained two time steps. First, blank-holder force (BHF) was applied and after that, displacement of punch was initialized and was kept until the forming process was finished. To establish the contact between the different parts, the surface to surface contact was used. The friction coefficients between die parts and blank have been obtained experimentally, and it is assumed that the contact property between the blank and die parts obeyed the coulomb's law. The friction coefficients of 0.23, 0.2 and 0.18 were applied for contact between blank with punch, blank-holder and die, respectively. To reduce the computation time, the die, punch and blank-holder were assumed to be rigid parts, and they were meshed with 3-D bilinear rigid quadrilateral elements. The circular blank sheet was meshed by explicit shell element SC8R with dividing it by 112 equal sectors and 18 equal segments along radius of the disc.

4. Validation of finite element analysis

4.1. *Experimental tests on the FML*

4.1.1. *Three-point bending test*

As aforementioned, standard specimens for three-point bending test of the FML were prepared according to the ASTM: D790 and the tests were performed using Zwick/Z250 testing machine. The desired standard dimensions of specimens were 76 × 15 × 2 mm, radii of supports and loading nose were 5 mm, and support span was 26 mm. The tests for several specimens were conducted at an ambient temperature of 25°C.

4.1.2. *Deep drawing test*

Deep drawing tests of laminates were carried out using a 60-tonne hydraulic press and a die set with blank-holder as shown in Figure 6. To measure the force of forming process and the displacement of punch, pressure transmitter and linear magnetic displacement sensor were installed on the press. The die and cylindrical punch with 70 mm and 64.5 mm diameters were made of SPK steel. The blank-holder and other parts of the die were made of MO40 and CK45 steel, respectively. The force of blank-holder was provided using eight B/32/051 springs with the same free length of 51 mm and $K = 134$ N/mm that were installed around the blank-holder. Deep drawing tests of the FMLs were performed at two different BHFs, i.e. 2.7 and 13 kN. No lubricant was used during the experiments and several specimens were tested for each BHF at an ambient temperature of 30°C.

4.2. *Results of the FE analysis*

4.2.1. *Three-point bending*

Figure 7(a) shows the deformed shape of the GFRP-based FML after the experiments. There was no visible fracture but delamination occurred at the composite/aluminum interface. This phenomenon shows that delamination is more critical than fracture in failure of the FMLs. Moreover, it shows that there is less resistance for adhesive against existent shear stress between layers due to continuing pressure of the loading nose. Deformed shape of the FML after simulation of three-point bending test is shown in Figure 7(b).

Figure 8 compares experimental and numerical force–displacement curves of the FML in the flexural test. There is a good agreement between the experimental and numerical results in most parts of the curves; however, the differences between the results increase after deflection of 2.5 mm. It can be attributed to the delamination and composite ply damage of the GFRP-based FML, which could not be predicted by the

Table 3. Dimensions of die parts.

	Die diameter	Punch diameter	Outer diameter of blank-holder	Inner diameter of blank-holder	Fillet of die	Fillet of punch
Amount (mm)	70	64.5	160	75	9	6

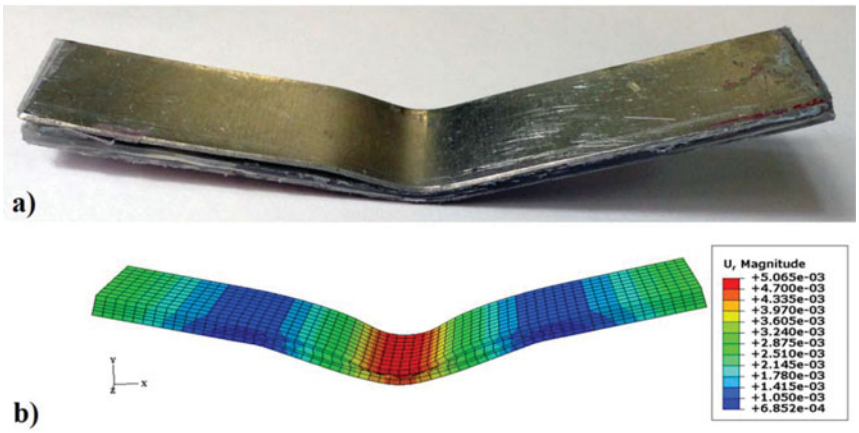

Figure 7. The deformed shapes of the FMLs after three-point bending test, (a) experimental and (b) numerical simulations.

present simulation. Prediction of damage needs to include a damage mechanism in the FML simulation model. The cohesive zone model (CZM) [22] is a proper candidate for prediction of delamination phenomena [23]. The force–displacement curve which is the output of testing machine can be transferred to stress-strain curve. Putting the force measured by device into the Eq. (4) gives the maximum axial stress, σ, at the midpoint of the beam, where P is the force applied to the sample, L is the support span, h is the sample thickness and b is the sample width. Furthermore, strain can be calculated using the displacement of the nose as shown in Eq. (5).

$$\sigma = \frac{3PL}{2bh^2}, \tag{7}$$

$$\varepsilon = \frac{6dh}{L^2}, \tag{8}$$

where ε is the longitudinal strain in the outer surface at midpoint of the beam and d is the midspan deflection of the beam. Figure 9 shows the stress-strain curves of the FML in tensile and flexural tests. As shown in the figure, in spite of fact that the tensile strength of the GFRP-based FML is 50 MPa, flexural strength of this material is higher, i.e. 66 MPa. This phenomenon can be attributed to this fact that the strength is controlled by distributed critical defects, whereas a much larger volume of material in a tension test is subjected to the maximum stress, hence, the probability of a critical defect increases and the strength decreases [24].

4. 2. 2. *Deep drawing*

The deep drawing tests of the FML were carried out to investigate the punch force–displacement curve and the various modes of failure in this process. Tearing and fracture are two modes of failure, which occur during deep drawing process. One of the other primary modes of failure in the deep drawing process is wrinkling. Unlike tearing and fracture, prediction of wrinkling within the deep drawing process is difficult and it is not determined from the force–displacement curve, while onset of tearing or fracture can be detected as a drop in the force–displacement curve. BHF has a significant effect on the failure modes of the FMLs; Lower BHF can cause wrinkling, whereas higher BHF can lead to tearing or fracture. Figure 10 shows laminates subjected to different BHFs. It can be seen that wrinkling and tearing are dominant at the BHFs of 2.7 and 13 kN, respectively.

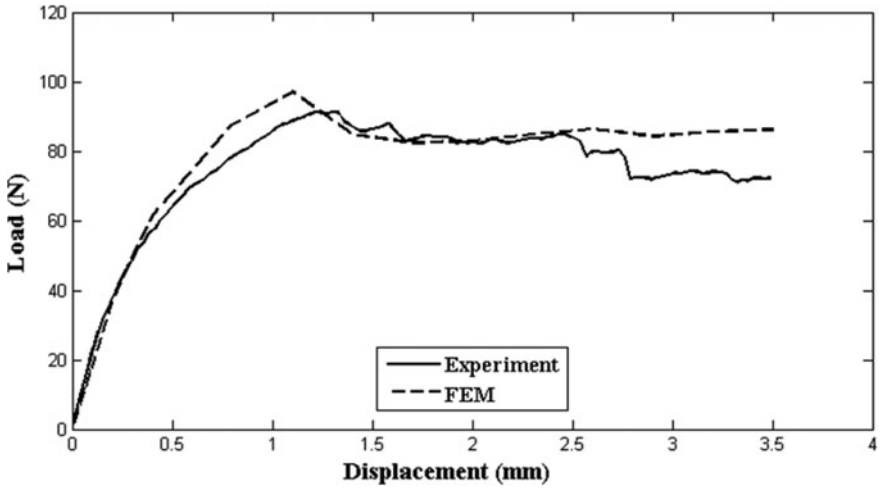

Figure 8. Validation of flexural load–displacement curve.

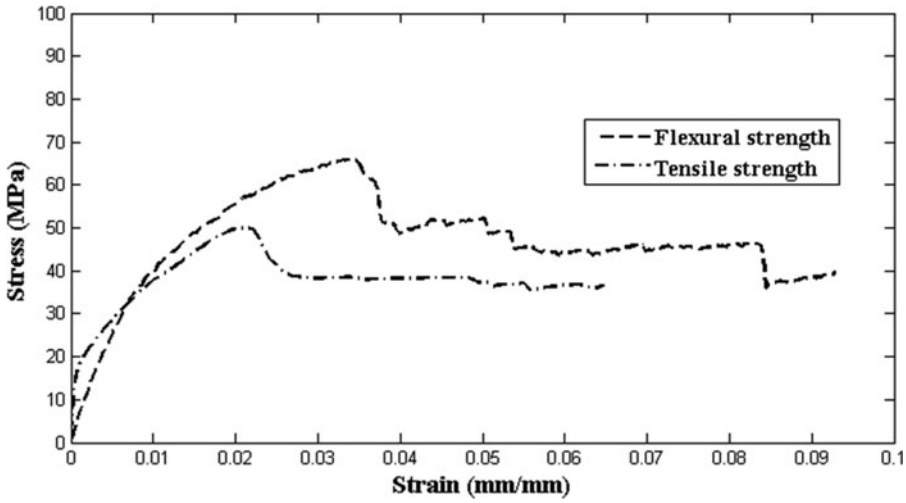

Figure 9. Tensile and flexural stress-strain curve of the beam (flexural strength was measured in the outer surface at midpoint).

Figure 10. Effect of blank-holder force (BHF) on the deformed FML specimens.

Figure 11 shows the experimentally and numerically deformed shapes of the FML with the BHF equal to 2.7 kN. This result revealed that FE analysis is capable of predicting failure mode of wrinkling within the deep drawing process and the location of wrinkles can be successfully predicted by FE analysis, which is in a good agreement with the experimental results.

Punch force–displacement curve is one of the most important parameters to study the deep drawing processes. It indicates several features of the process, including required force, depth of drawing and the onset of failure by tearing or fracture. The depth at which the failure occurred during the forming process was used as a measure of the formability of a laminate. Figure 12 shows the obtained experimental and numerical results for force–displacement curves of the both specimens in Figure 10. The comparison between the results shows that the experimental curves follow the same trend with those of predicted by simulations with a good accuracy. In deep drawing process, increasing of blank holder force increases the friction and in turn the required punch force. As indicated in Figure 12, drawing force of 13 kN BHF sample is higher than that of 2.7 kN BHF one for each drawing depth. Moreover, the sample with 13 kN BHF has approximately 17 mm draw depth, while the other sample with 2.7 kN BHF reaches the maximum draw depth of 25 mm.

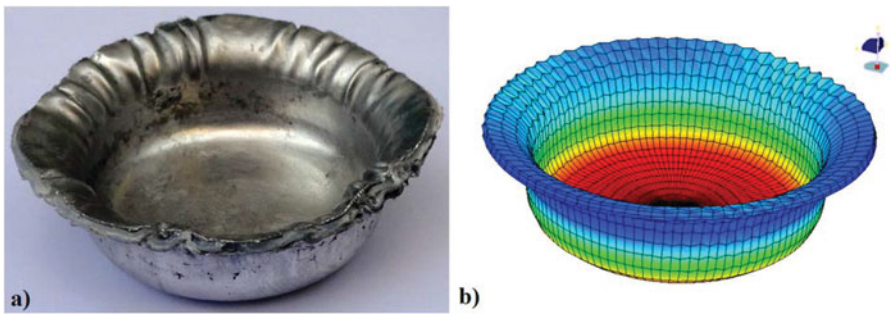

Figure 11. Comparison between the drawn FML samples, (a) experimental and (b) numerical simulations.

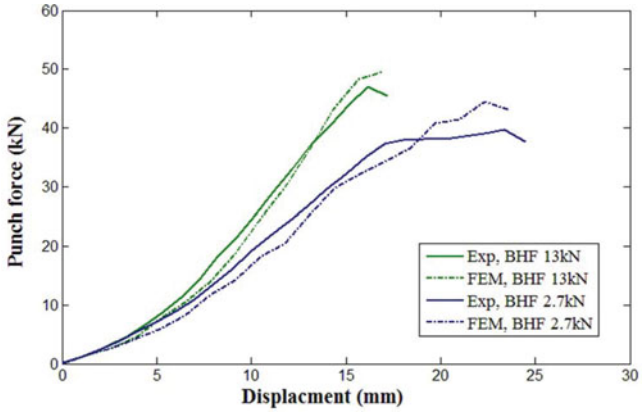

Figure 12. Validation of punch force–displacement curves for different BHFs.

5. Conclusions

In this article, the bending and the drawing behaviors of the GFRP-based FML were investigated. FE analysis was used as a numerical approach to predict the prescribed mechanical behaviors of this material. A practical method was introduced for determination of directional properties in the orthotropic composite based on Timoshenko's beam theory. The obtained engineering constants can be used for simulation of various types of the mechanical tests on this FML. In order to validate the accuracy of FE analysis, some experimental tests were carried out. Comparison of the results showed that FEA successfully predicted the occurrence and location of wrinkling. Moreover, force–displacement curves of three-point bending and deep drawing tests in two methods were in a good agreement. The results showed the effectiveness of the method used for obtaining directional properties of the FML.

References

[1] G. Reyes and H. Kang, J. Mater. Process. Technol., vol. 186, pp. 284–290, 2007.
[2] G. Reyes and S. Gupta, Composites Part A: Appl. Sci. Manuf., vol. 40, pp. 176–183, 2009.
[3] J.G. Carrillo and W.J. Cantwell, Mech. Mater., vol. 41, pp. 828–838, 2009.
[4] S.E. Moussavi-Torshizi, S. Dariushi, M. Sadighi, and P. Safarpour, Mater. Sci. Eng: A, vol. 527, pp. 4920–4925, 2010.
[5] S.M.R. Khalili, R.K. Mittal, and S.G. Kalibar, Mater. Sci. Eng: A., vol. 412, pp. 137–140, 2005.
[6] J. Gresham, W. Cantwell, M.J. Cardew-Hall, P. Compston, and S. Kalyanasundaram, Compos. Struct., vol. 75, pp. 305–312, 2006.
[7] C.T. Lin, P.W. Kao, and F.S. Yang, Composites, vol. 22, pp. 135–141, 1991.
[8] J. Macheret and R.J. Bucci, Eng. Fract. Mech., vol. 45, pp. 729–739, 1993.
[9] J. Mackerle, Comput. Mater. Sci., vol. 31, pp. 187–219, 2004.
[10] M.H. Parsa, S. Nasheralahkami, and M. Ettehad, Mater. Des., vol. 31, pp. 4174–4183, 2010.
[11] J. Fan, Z.W. Guan, and W.J. Cantwell, Compos. Struct., vol. 93, pp. 2430–2436, 2011.
[12] L. Mosse, P. Compston, W.J. Cantwell, M. Cardew-Hall, and S. Kalyanasundaram, Compos. Struct., vol. 75, pp. 298–304, 2006.
[13] J.Y. Zheng and P.F. Liu, Comput. Mater. Sci., vol. 42, pp. 453–461, 2008.
[14] A. Derewońko, Comput. Mater. Sci., vol. 45, pp. 735–738, 2009.
[15] T. Kaneko, J. Phys. D: Appl. Phys., vol. 8, pp. 1927–1936, 1975.
[16] G.J. Kennedy, J.S. Hansen, and J.R.R.A. Martins, Int. J. Solids Struct., vol. 48, pp. 2373–2382, 2011.
[17] S.P. Timoshenko, Philos. Mag., vol. 43, pp. 125–131, 1922.
[18] G. Caprino, P. Iaccarino, and A. Lamboglia, Compos. Struct., vol. 88, pp. 360–366, 2009.
[19] J.M. Berthelot and J.M. Cole, Composite Materials: Mechanical Behavior and Structural Analysis, Springer, New York, 1998.
[20] P. Xu, J.Y. Zheng, and P.F. Liu, Mater. Des., vol. 30, pp. 2295–2301, 2009.
[21] Abaqus User's Examples and Theory Manuals. Dassault Systemes Simulia Corp., Providence, RI, USA, 2010.
[22] I.A. Ashcroft, Z.R. Khokar, and V.V. Silberschmidt, Comput. Mater. Sci., vol. 52, pp. 95–100, 2012.
[23] M. Parsa and M. Ettehad, In: D. Yang (Ed.) The 9th International Conference on Technology of Plasticity, Korea, 2008, pp. 980–985.
[24] M.R. Wisnom, J. Compos. Mater., vol. 28, pp. 1173–1180, 1992.